

# Prediction of Specific Biomolecule Adsorption on Silica Surfaces as a Function of pH and Particle Size

Fateme S. Emami,<sup>†</sup> Valeria Puddu,<sup>‡</sup> Rajiv J. Berry,<sup>§</sup> Vikas Varshney,<sup>§</sup> Siddharth V. Patwardhan,<sup>||</sup> Carole C. Perry,<sup>\*,‡</sup> and Hendrik Heinz<sup>\*,†</sup>

<sup>†</sup>Department of Polymer Engineering, University of Akron, Akron, Ohio 44325-0301, United States

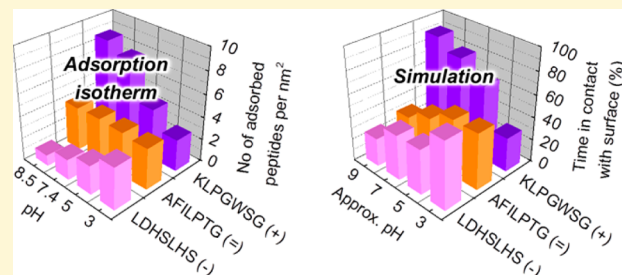
<sup>‡</sup>Interdisciplinary Biomedical Research Centre, School of Science and Technology, Nottingham Trent University, Clifton Lane, Nottingham NG11 8NS, United Kingdom

<sup>§</sup>Materials and Manufacturing Directorate, Air Force Research Laboratory, Wright-Patterson Air Force Base, Wright-Patterson Air Force Base, Ohio 45433, United States

<sup>||</sup>Department of Chemical and Process Engineering, University of Strathclyde, 75 Montrose Street, Glasgow G1 1XJ, United Kingdom

## Supporting Information

**ABSTRACT:** Silica nanostructures are biologically available and find wide applications for drug delivery, catalysts, separation processes, and composites. However, specific adsorption of biomolecules on silica surfaces and control in biomimetic synthesis remain largely unpredictable. In this contribution, the variability and control of peptide adsorption on silica nanoparticle surfaces are explained as a function of pH, particle diameter, and peptide electrostatic charge using molecular dynamics simulations with the CHARMM-INTERFACE force field. Adsorption free energies and specific binding residues are analyzed in molecular detail, providing experimentally elusive, atomic-level information on the complex dynamics of aqueous electric double layers in contact with biological molecules. Tunable contributions to adsorption are described in the context of specific silica surface chemistry, including ion pairing, hydrogen bonds, hydrophobic interactions, and conformation effects. Remarkable agreement is found for computed peptide binding as a function of pH and particle size with respect to experimental adsorption isotherms and  $\zeta$ -potentials. Representative surface models were built using characterization of the silica surfaces by transmission electron microscopy (TEM), scanning electron microscopy (SEM), Brunauer–Emmett–Teller (BET), thermalgravimetric analysis (TGA),  $\zeta$ -potential, and surface titration measurements. The results show that the recently introduced interatomic potentials (Emami et al. *Chem. Mater.* 2014, 26, 2647) enable computational screening of a limitless number of silica interfaces to predict the binding of drugs, cell receptors, polymers, surfactants, and gases under realistic solution conditions at the scale of 1 to 100 nm. The highly specific binding outcomes underline the significance of the surface chemistry, pH, and topography.



## 1. INTRODUCTION

Silicon dioxide, or silica, is widely available in mineral form, biologically enriched in organisms, and produced by laboratory synthesis.<sup>1–3</sup> It is extensively used as a filler material in nanocomposites and tires and in separation media for liquids and gases, cosmetics, catalyst supports, and building materials. Porous silica nanoparticles that exploit specific interactions with biological molecules in aqueous solution are also used in drug delivery systems, biomarkers, sensors, and nanoreactors.<sup>4–10</sup> The performance for this broad range of applications is often still evaluated by trial and error and results remain difficult to explain. For example, efforts to synthesize silica from precursors to replicate hierarchically organized silica-protein skeletons similar to diatoms, marine organisms,<sup>5,11,12</sup> and plants have shown first successes in achievable structural order.<sup>7,9,13–17</sup> However, fundamental insight into mechanisms and control of assembly remains incomplete even though many amino acid

sequences, peptides and proteins from microorganisms, cellular templates, and designed ligands have been tested.<sup>6–10,14,18</sup>

Therefore, better understanding of the role of the precursors, of the surface chemistry of silica formed, as well as of the competitive interactions with solvents and proteins could provide significant benefits to the rational engineering of silica-based materials. The effect of synthesis conditions, pH, buffer composition, and molecular conformation on materials formation is known to be critical.<sup>9,19,20</sup> However, limitations of current laboratory instrumentation pose difficulties to answer questions related to silica biominerization and specific molecular recognition at the scale of 1 to 100 nm where complementary guidance from simulations can be very helpful.<sup>9,18,21–36</sup>

Received: July 22, 2014

Revised: August 25, 2014

Published: August 26, 2014



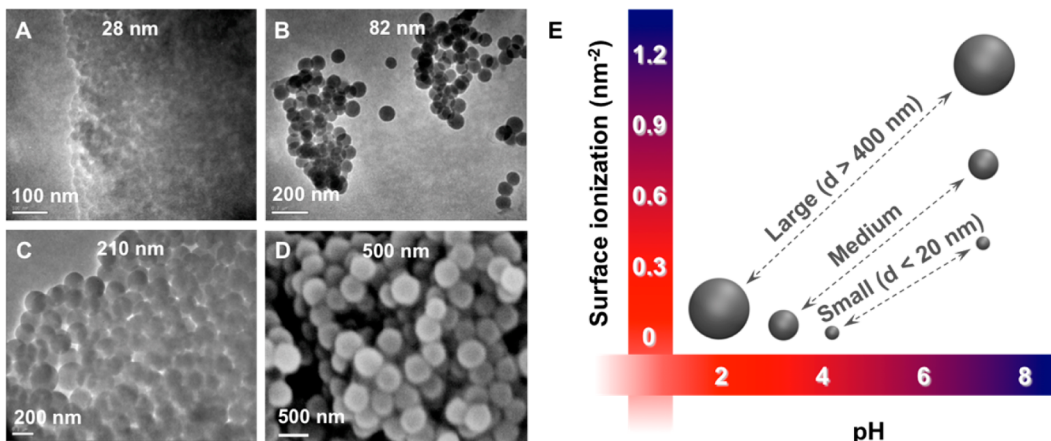


**Figure 1.** Electron microscopy images of amorphous silica nanoparticles of different size from Stöber-type synthesis, and the effect of pH and particle size on surface ionization (from refs 37 and 42). (A–D) TEM and SEM images for nanoparticles of average sizes 28, 82, 210, and 500 nm (ref 42). Silica nanoparticles of size 28 nm are less dense and poorly defined in comparison to spherical larger particles. (E) Schematic relationship between surface ionization, pH, and particle size. Large nanoparticles contain  $Q^2/Q^3$  surface environments, medium size and smaller nanoparticles contain mostly  $Q^3$  environments. The amount of  $\text{SiO}^- \text{Na}^+$  groups per  $\text{nm}^2$  is shown at an ionic strength of 0.1–0.3 mol·dm<sup>-3</sup> (see further details in SI Table S1 and original data in refs 9, 38–41).

**Table 1. Sequence, Charge, Isoelectric Point, and Hydrophilicity of the Selected Peptides, Identified by Phage Display<sup>10</sup>**

Peptide name	Sequence	Net charge at pH=7.4	pI	Hydrophilicity <sup>a</sup>
S1	<b>K<sup>+</sup>LPGWSG · Cl<sup>-</sup></b>	+1	9.8±0.2	-0.3
S2	<b>A<sup>+</sup>FILPTG</b>	0	5.8±0.2	-1
S3	<b>LD<sup>+</sup>HSLHS · Na<sup>+</sup></b>	-1	6.1±0.1	-0.1

<sup>a</sup>Values close to zero correspond to hydrophilicity while values close to -1 correspond to hydrophobicity. Calculated according to ref 42.

Studies by biopanning and molecular simulation with the polymer consistent force field (PCFF) extended to silica recently identified a range of contributions to specific adsorption of peptides on amorphous silica particles.<sup>9,10,26</sup> These contributions include ion pairing between positively charged groups in the peptides and negatively charged siloxide groups on the silica surface ( $\equiv\text{SiO}^- \cdots \text{Na}^+$ ) accompanied by neutralization of the  $\zeta$ -potential, hydrogen bonds, van-der-Waals interactions with the surface, and conformation effects. The significance of each of these adsorption modes was found to depend on experimental conditions such as pH, peptide sequence, and silica surface chemistry. As a consequence, the nature and strength of the interactions can only be identified using dedicated molecular models that closely represent the experimental conditions.

The aim of this contribution is the atomic-scale visualization of the binding process and quantitative predictions of specific adsorption of peptides to all types of silica surfaces using computer simulations. A companion paper recently introduced accurate force field parameters and a detailed surface model database for silica,<sup>37</sup> which are employed here in the form of the CHARMM-INTERFACE force field.<sup>26</sup> This study focuses on the effects of pH and particle size that modulate ionization, surface structure, and specific peptide adsorption (Figure 1).<sup>9,38–41</sup> The chosen peptides include consensus silica binding sequences composed of seven amino acids with different net charge (-1, 0, +1) and hydrophilicity that were previously identified by phage display (Table 1).<sup>10</sup> The chosen nanoparticles are of diameters 28 nm, 82 nm, and 210 nm, and have undergone characterization of their surface chemistry by Brunauer–Emmett–Teller (BET), Barrett–Joyner–Halenda

(BJH), thermogravimetric analysis (TGA), transmission electron microscopy (TEM), scanning electron microscopy (SEM), and  $\zeta$ -potential measurements (Figure 1).<sup>42</sup>

The outline of this paper is as follows: The recently introduced force field and surface model database for silica interfaces are briefly reviewed (section 2). Specific peptide adsorption, binding free energies, and mechanisms of interaction with silica surfaces are described as a function of pH and particle size, thereby illustrating the predictive detail of simulations (section 3). A summary of the major results and conclusions follows at the end (section 4). The Supporting Information (SI) provides full details of computational and experimental methods, experimental data employed for validation, as well as further information (SI sections S1 to S4).

## 2. RECENT DEVELOPMENTS IN MODELING AND SIMULATION OF SILICA INTERFACES

Recently, a companion paper introduced a force field and a surface model database for silica to simulate bulk, surface, and interfacial properties in atomic resolution.<sup>37</sup> This work explains chemical bonding and surface features of silica in depth to enable quantitative studies of silica–biomolecular interfaces at the scale of 1 to 100 nm under realistic solution conditions. Major improvements in the force field include the chemically consistent representation of ionic versus covalent bonding in silica, incorporation of full details of surface chemistry, surface ionization, as well as validation of interfacial properties in ~5% agreement with experiment, down from up to 500% error previously.<sup>26,37</sup> Prior force fields often required fixed atoms to avoid collapse of the models in the simulation, neglected the

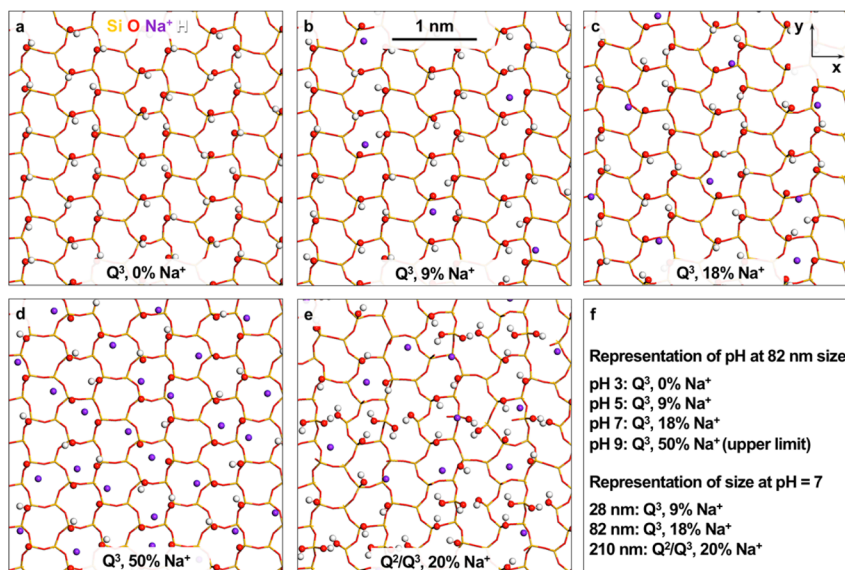
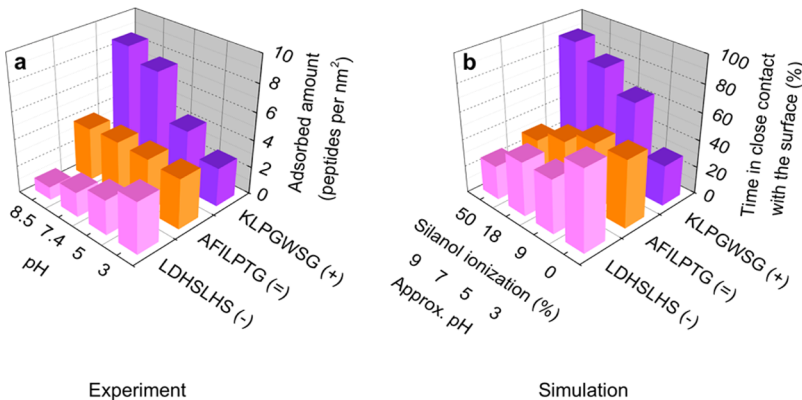


**Figure 2.** Silica model surfaces for different pH and particles of different size in top view. (a–d) Regular  $Q^3$  surfaces with 4.7  $\text{SiO}(\text{H}, \text{Na})$  groups per  $\text{nm}^2$  and different amount of  $\text{SiO}^- \text{Na}^+$  groups represent pH values of 3, 5, 7, and 9 for 82 nm size nanoparticles. (e) The regular  $Q^2/Q^3$  surface with 6.5  $\text{SiO}(\text{H}, \text{Na})$  groups per  $\text{nm}^2$  and 20% ionization represents 210 nm size particles at pH 7. High area density of both  $\text{SiOH}$  and of  $\text{SiO}^- \text{Na}^+$  groups results in stronger adsorption of all peptides. Models for particles of 28 and 82 nm size at pH 7 correspond to b and c. (f) Summary of correspondence of chosen models to pH and particle size near physiological ionic strength.



pH dependence of the surface chemistry, and involved other drastic approximations so that even approximate predictions of specific binding of biomolecules were very difficult.<sup>43–56</sup>

The new, thermodynamically consistent silica parameters are compatible with comprehensive harmonic force fields for biopolymers, organic molecules, and inorganic compounds such as CHARMM, AMBER, PCFF, COMPASS, CVFF, and INTERFACE.<sup>26,37</sup> The compatibility enables insight into a limitless number of silica hybrid materials by the possible combination of thousands of distinct silica surface structures with billions of distinct biopolymers, surfactants, and receptor molecules across a wide range of concentrations and solution conditions. A surface model database covers experimentally observed surface chemistries of all types of silica and aids in the preparation of customized nanostructures for given conditions (SI Table S1).<sup>37</sup>

The novel features of the force field and of the surface model database are summarized more inclusively as follows: (1) full

atom mobility, (2) reproduction of the lattice parameters of crystalline silica ( $\alpha$ -quartz,  $\alpha$ -cristobalite), (3) coverage of the full range of surface chemistry with  $Q^2$ ,  $Q^3$ ,  $Q^4$ , amorphous, and porous environments, (4) coverage of the full range of surface ionization corresponding to surface type and pH, (5) agreement of computed immersion energies, contact angles of water, and adsorption isotherms with laboratory measurements (using common SPC and TIP3P water models), (6) correlation of cation dissociation with measured  $\zeta$ -potentials as a function of pH and nanoparticle size, (7) full compatibility with many harmonic energy expressions (see above). These features are described in ref 37. The present contribution illustrates that the accurate reproduction of the structure and interfacial properties of pristine silica provides also a solid foundation for realistic simulations of silica–organic and silica–biomolecular interfaces. The improvements in accuracy up to 2 orders of magnitude over earlier models<sup>9,32,53,57–64</sup> result from the careful implementation and interpretation of chemical details

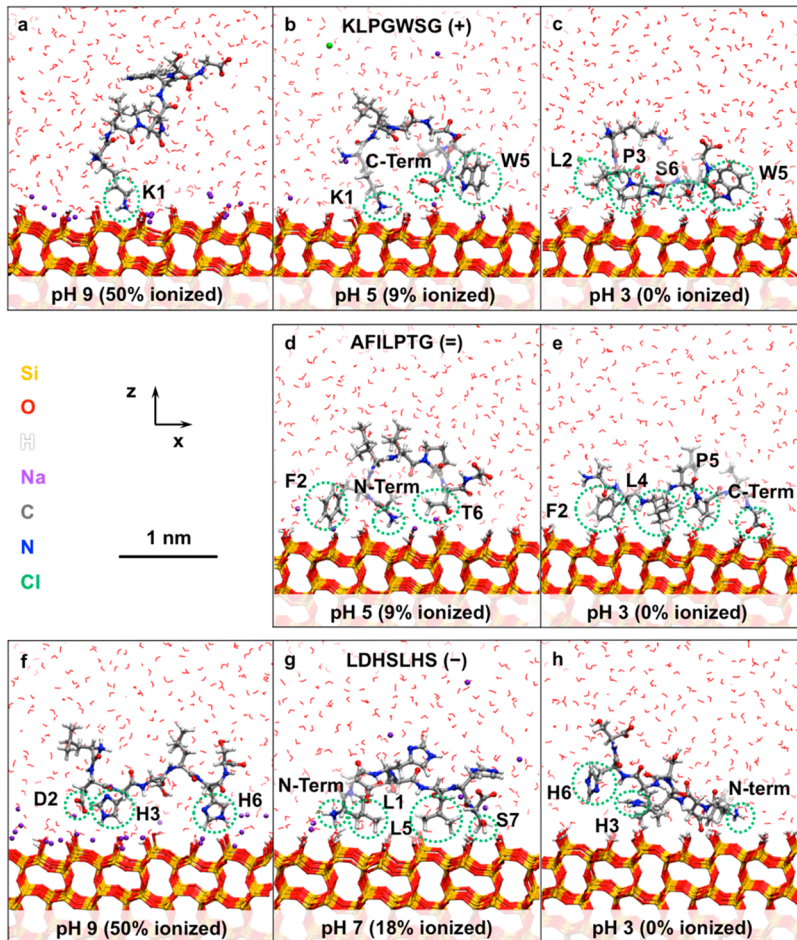


**Figure 4.** Selected conformation of three peptides of different charge on  $Q^3$  silica surfaces for a series of pH values according to simulation. The surfaces represent silica particles of 82 nm size with 4.7  $\text{SiO}(\text{H}, \text{Na})$  groups per  $\text{nm}^2$  and variable ionization. (a–c) The positively charged peptide KLPGWSG, (d,e) the overall neutral peptide AFILPTG, (f–h) the negatively charged peptide LDHSLHS. Amino acid residues with significant surface interactions are highlighted. Close contact with the surface as shown occurs between >90% (a) and 20% (f) of time depending on affinity.

in the INTERFACE force field,<sup>26</sup> as also shown for other inorganic–organic interfaces.<sup>9,21,25,29,30,65–72</sup>

### 3. RESULTS AND DISCUSSION

#### 3.1. Specific Peptide Adsorption as a Function of pH.

The three peptides shown in Table 1 and silica nanoparticles of 82 nm uniform size (Figure 1b) were chosen to investigate the impact of pH on specific peptide adsorption. Extensive experimental characterization of the silica surfaces by BET, TGA, and  $\zeta$ -potential measurements as well as of peptide adsorption by adsorption isotherms is available (SI Figures S1 to S3).<sup>10,42</sup> The nanoparticle surfaces at pH values of 3, 5, 7.4, and 8.5 were represented by regular  $Q^3$  silica surfaces with specific degrees of ionization of silanol groups  $\equiv\text{Si}–\text{OH}$  to siloxide groups  $\equiv\text{SiO}^–\cdots \text{Na}^+$  (Figure 2).<sup>10</sup> The degrees of ionization are 0%, 9%, 18%, and 50%, respectively, for the pH values mentioned above (see details in SI Table S1).<sup>37</sup> The chemical appearance of these surfaces differs significantly, leading to an amount of dissociated cations of 0, 0.27, 0.45, and 0.30 cations per  $\text{nm}^2$ , whereby the value of 50% silanol ionization corresponds to maximum ionization of the silica surface somewhat above pH 8.5.<sup>37</sup> The pH values of the peptides were represented in the models by the appropriate charge state of pH-sensitive residues (N-terminus, K, D, H, C-

terminus) and addition of oppositely charged ions to maintain overall charge neutrality when needed ( $\text{Na}^+, \text{Cl}^-$ ).

Large-scale parallel molecular dynamics simulations of the three peptides on the silica surfaces were then carried out, including multiple independent start conformations, thermal annealing, and total simulation times in excess of 20 ns (Figures 3 and 4; see details in SI section S1).<sup>73</sup> A very good correlation between the amount of adsorbed peptides according to the adsorption isotherms (Figure 3a)<sup>10</sup> and the percentage of time close to the surface in the simulations was observed (Figure 3b) without further assumptions. Close contact of the peptides was thereby defined as a distance of less than 3 Å from the surface oxygen atoms. Computed adsorption energies  $\Delta E_C$  and computed adsorption free energies  $\Delta F_C$  also correlate with the adsorbed amount of peptide in experiment (Table 2). Values below zero correspond to attraction and a larger amount adsorbed. Nearly equal values of adsorption energies and adsorption free energies are notable, whereby computed adsorption free energies are shown only for the cationic peptide KLPGWSG due to the high computational cost of umbrella sampling and steered MD (Table 2 and SI section S1). Using the relation  $\Delta F_C = \Delta E_C - T\Delta S_C$ , it is found that net entropic contributions to adsorption  $-T\Delta S_C$  are small, essentially within the uncertainty of  $\pm 2$  kcal/mol. Therefore, the adsorption energy  $\Delta E_C$  is a good first approximation for the

**Table 2. Computed Energy of Adsorption of the Peptides on Q<sup>3</sup> Silica Surfaces of Different pH Value According to Molecular Dynamics Simulation ( $\pm 2$  kcal/mol)<sup>a</sup>**

peptide (charge at pH 7)	adsorption energy (kcal/mol)			
	pH ~ 3 (0% ionized)	pH ~ 5 (9% ionized)	pH ~ 7.4 (18% ionized)	pH > 8.5 (50% ionized)
KLPGWSG (+)	-1	-1	-3	-7
KLPGWSG (+) free energy	0	-1	-6	-8
AFILPTG (=)	+3	+1	+3	+4
LDHSLHS (-)	-2	+1	+2	+4

<sup>a</sup>Computed free energies of adsorption are also shown for KLPGWSG ( $\pm 0.5$  kcal/mol).

free energy of binding  $\Delta F_C$  of short peptides. Similar suggestions have been made previously for the binding of peptides on metal and silica surfaces in aqueous solution.<sup>9,22,67,73</sup> The present quantitative data therefore confirm a certain entropy loss of the peptide upon adsorption due to decreased conformational freedom, which is compensated, or slightly overcompensated, by the release of surface-bound water that gains translational and rotational mobility. Computed binding free energies  $\Delta F_C$  of 0, -1, -6, and -8 kcal/mol ( $\pm 0.5$  kcal/mol) on 0%, 9%, 18%, and 50% ionized surfaces also agree with binding free energies  $\Delta F_A$  in a range from -4 to -7 kcal/mol for peptide KLPGWSG derived from the adsorption isotherms (SI Table S2). The experimental values  $\Delta F_A$  were derived from approximate binding constants  $K_A$  according to  $\Delta F_A = -RT \ln K_A$ , whereby uncertainties are also difficult to reduce below  $\pm 2$  kcal/mol (SI section S1.4).<sup>10</sup> In addition, computed adsorption energies correlate with the experimental threshold concentration of peptides to achieve significant adsorption (SI Figure S4 and SI section S3).

A major benefit from the simulation is the access to structural information on the atomic scale (Figure 4, Table 3, and SI Movie S1). Visualizations (Figure 4 and SI Movie S1) and time-averaged information on the proximity of individual residues and residence times on the surface (Table 3) explain the mechanism of selective adsorption. The positively charged peptide KLPGWSG is more attracted to surfaces at higher pH, which carry an increased negative charge per area (Figure 3). On the 50% and 18% ionized surfaces, that is, at pH 9 and 7, the peptide is anchored to the surface by the ammonium groups of the N-terminal and the K1 side chain for more than 80% of the time (Figure 4a). At lower ionization of 9% and 0%, that is, at pH 5 and 3, electrostatic interactions through ion pairing are diminished and hydrogen bonds of the OH groups of S6 and of ammonium groups on N-terminal K1 with the silica surface increasingly contribute to adsorption (Figure 4b, c). In addition, close contacts of L2, P3, and W5 side chains with the surface are seen (Table 3). Hydrophobic residues have thereby no intrinsic affinity to the silica surface; their surface attachment mainly diminishes disruptions of the hydrogen-bonded structure of liquid water, equal to a reduction in excluded volume. Near-neutral silica surfaces therefore attract hydrophobic residues to concentrate unfavorable hydrophobic (van der Waals) interactions directly at the surface; however, hydration shells of siloxide ions and cations on ionized silica surfaces keep hydrophobic residues away. The time-averaged adsorbed conformation of the positively charged peptide KLPGWSG, therefore, changes from anchor-like with strong contribution by ammonium groups on highly negatively

**Table 3. Adsorption Strength of Peptides Bound to Q<sup>3</sup> Silica Surfaces at Different pH Values, Characterized by the Percentage of Simulation Time in Close Contact with the Surface, That Is, <3 Å Vertical Distance from the Superficial Layer of Silanol Oxygen Atoms<sup>a</sup>**

peptide	pH ~ 3 (0% ionized)		pH ~ 5 (9% ionized)		pH ~ 7 (18% ionized)		pH > 8.5 (50% ionized)	
	time %	closest residues	time %	closest residues	time %	closest residues	time %	closest residues
KLPGWSG (+)	30	W5, K1, N-terminal, P3, S6 (hydrophobic interactions dominate at lower ionization)	65	N-term, K1 $\gg$ C term > L2, W5, P3	75	N-term, K1 $\gg$ C-term, S6 $\gg$ P3, W5, L2	90	N-term, K1 $\gg$ C-term > S6, W5
AFILPTG (=)	50	N-term, C-term, T6, F2, L4, I3, P5	50	N-term > C-term, T6, F2, L4, I3, P5	40	N-term > C-term, T6, F2, L4, I3, P5	30	N-term > C-term, T6 > F2 > I4, I3
LDHSLHS (-)	60	N-term, C-term, S7, D2, S4, H3, H6, L1, L5	40	N-term, C-term, S7, D2, S4, H3, H6, L1, L5	40	N-term, C-term > S7, D2, S4, H3, H6, L1, L5	20	N-term, C-term > S7, D2, S4, H3, H6, L1, L5

<sup>a</sup>Amino acids are ranked in the order of proximity to the surface with the closest first. Statistical uncertainties in time averages are  $\pm 5\%$ .

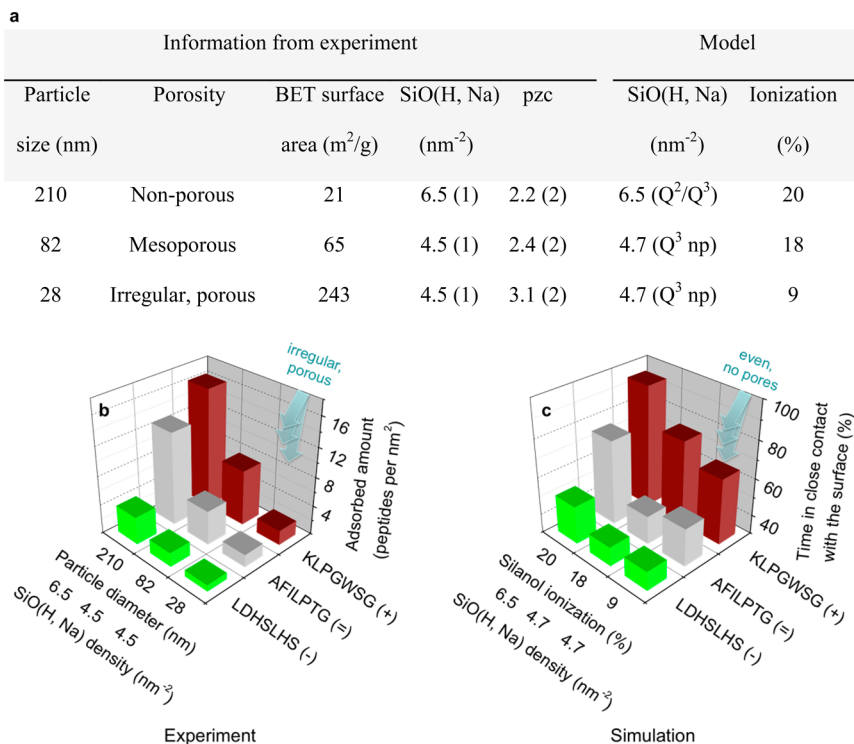


**Figure 5.** Surface characteristics of silica nanoparticles of different size and adsorption of peptides in experiment and simulation at pH = 7.4. (a) Nanoparticle characteristics (from ref 42) and corresponding model assumptions (np = nonporous). (b) Adsorbed amount of three differently charged peptides per BET surface area at 1 mM initial peptide concentration as a function of nanoparticle size in experiment. (c) Percentage of time that peptides are in direct contact with the surface (<3 Å) in the simulation. The agreement is good, and the high impact of irregularity on adsorption is seen for the 28 nm particles (poor particle definition in experiment b versus ideal regular surfaces in simulation c).

charged surfaces (Figure 4a) to flat-on arrangements with higher mobility (Figure 4c) and more contact of polar and hydrophobic functional groups on less ionized surfaces (L2, P3, W5).

Adsorption of the overall neutral peptide AFILPTG was weaker than for KLPGWSG and statistically not affected by changes in surface ionization and pH (Figure 3). Interactions with the 50% ionized surface, which exceed the experimental surface charge, were found to be slightly more repulsive than in experiment (Table 3). On all other surfaces, the peptide was in contact with the silica surface at least 40% of the simulation time through the N-terminal ammonium group by electrostatic forces (ion pairing) as well as through hydrogen bonds that involve the carboxylate of the C-terminal and the OH group in T6 in contact with surface silanol groups (Figure 4d). Additional hydrophobic interactions were observed through the phenyl ring in F2, the L4 side chain, and the ring of P5 in agreement with experimental observations (Figure 4e and Table 3).<sup>10</sup>

The negatively charged peptide LDHSLHS showed less time in contact with most surfaces than the other two peptides and adsorption decreased with higher density of negative charge (Figure 3, Table 3). This peptide also notably changes its own charge from approximately -1.5 at pH 8.5 to +2 at pH 3.<sup>42</sup> Direct contact with the highly ionized surface at pH 8.5 amounted to only 20% of simulation time (Figure 4f) and increased to above 40% of simulation time for 18% and 9% ionized silica surfaces, respectively (Figure 4g). The N-terminus of L1 and hydroxyl groups in S7, as well as some hydrophobic groups approach the surface at lower pH (Table 3). At the point of zero charge, the peptide is in close contact with the

surface for more than 60% of simulation time, including protonated H3, H6, and temporarily all residues (Figure 4h and SI Movie S1).

In summary, molecular dynamics simulation with the new silica force field predicts peptide adsorption as a function of pH in remarkable correlation with experiment, and contributions to binding can be traced in atomic detail. It is shown that ion pairing, hydrogen bonds, and hydrophobic interactions, as well as conformation effects (especially for longer peptides and proteins) contribute to selective binding.<sup>9</sup> Electrostatic and polar interactions are thereby stronger than hydrophobic interactions. Hydrophobic interactions become significant at lower degree of surface ionization and involve many binding sites throughout the peptide chain, driven by the separation of hydrophobic groups from the aqueous phase onto the surface. The contribution of each binding mode can be quantified and visualized for specific surface conditions and biomolecules. Changes in proton distribution on the peptides such as across L1, D2, H3, H6, and S7 residues of LDHSLHS are also essential to understand selective adsorption as a function of pH. Future studies may also explore simulations with multiple adsorbed peptides corresponding to higher initial peptide concentration.

**3.2. Specific Peptide Adsorption as a Function of Silica Nanoparticle Size.** In this section, it is shown how the same approach can be applied to understand specific peptide binding to silica nanoparticles of variable size (Figure 1). Silica nanoparticles of different synthetic origin are generally distinguishable by differences in surface chemistry and topology and, in turn, attract highly dissimilar peptides.<sup>9,10,37,42,74</sup> A common example is Stöber-type silica nanoparticles of different

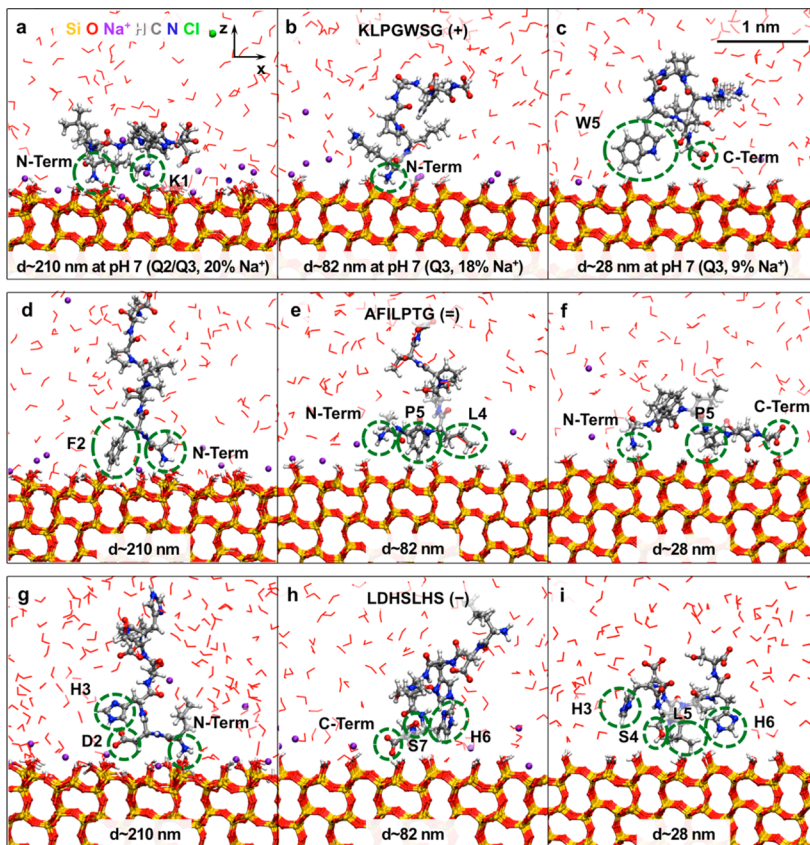


**Figure 6.** Selected conformations of three peptides of different charge on silica surfaces representing nanoparticles of 210, 82, and 28 nm sizes at pH  $\sim$  7. (a–c) The positively charged peptide KLPGWSG, (d–f) the neutral peptide AFILPTG, (g–i) the negatively charged peptide LDHSLHS. Amino acid residues with significant surface interaction are highlighted. The actual percentage of time in close contact with the surface varies between 90% (a) and 40% (e, h, and i) depending on affinity (see SI Table S3).

size that are produced using different amounts of ammonia to hydrolyze precursors and, in turn, attract peptides of less than 20% sequence similarity at the same pH value.<sup>9</sup>  $\zeta$ -potential measurements show that larger silica nanoparticles exhibit more surface ionization and a lower point of zero charge (Figure 1 and SI Figure S1), thus attracting peptides of higher positive charge (of higher isoelectric point pI).<sup>9,37,42</sup> Qualitatively, this relation was previously verified by molecular simulations, which showed that combinatorially selected peptides binding to 82 nm particles (pep 1, KSLSRHDHIHHH, pI 8.8) were less attracted to 450 nm particles, and combinatorially selected peptides binding to 450 nm particles (pep4, MHRSDLMSAAVR, pI 9.4) were less attracted to 82 nm particles.<sup>9</sup> The surfaces were then approximated as ionized  $Q^3$  environments for 82 nm particles and as ionized  $Q^2$  environments for 450 nm particles, respectively, using the PCFF-SILICA force field (please refer to SI Table S1 for details of the surface chemistry of silica particles of different chemistry and size).<sup>37</sup>

Recent further characterization by TEM, SEM, BET, BJH, TGA, XPS, and  $\zeta$ -potential measurements quantified size-dependent differences in surface chemistry, including the area density of silanol groups (silanol number), the degree of ionization, surface morphology, and porosity (Figure 5a, see details in SI section S2).<sup>42</sup> Therefore, silica nanoparticles of 28, 82, and 210 nm size and the same set of peptides as above (Table 1) were chosen to evaluate the influence of particle size on specific peptide adsorption at a constant pH value of 7.4 (Figure 5b). Quantitative affinity predictions by molecular

dynamics simulations are in good agreement with measurements (Figure 5c), although differences for poorly defined surfaces of 28 nm particles are also noted.

A critical aspect hereby is the use of realistic surface models. TEM and SEM measurements show the irregular, “spongy” structure of 28 nm nanoparticles in contrast to the well-developed spherical geometry of larger particles (Figure 1a–d). Due to the lack of specific enough information, regular surfaces were nevertheless assumed for simplicity. For 82 and 210 nm particles with some mesoporosity or negligible porosity, respectively, regular surface topography on the 5 nm scale is a good approximation. The total SiOH area density and surface acidity according to TGA and  $\zeta$ -potential measurements differ significantly (Figure 5a) and corresponding surface models were appropriately matched to the respective area density of silanol groups and degree of ionization (Figure 2). The small and medium size particles of 18 and 82 nm size were accordingly represented by regular  $Q^3$  surfaces with a silanol density of 4.7 groups per  $\text{nm}^2$  with 9% and 18% ionization, respectively, consistent with data about the point of zero charge (pzc) and surface titration (SI Table S1).<sup>9,38–41</sup> The nanoparticles of 210 nm size were represented by a mixed  $Q^2/Q^3$  surface with a silanol density of 6.5 groups per  $\text{nm}^2$  and 20% ionization, accounting for higher silanol density and lower pzc. The cation density per unit area was thus 54% higher in 210 nm particles than in 82 nm particles. Nanoparticles of 500 nm size could also be represented by the same mixed  $Q^2/Q^3$  surface with  $\sim$ 30% ionization (2.0  $\text{SiO}^- \text{Na}^+$  groups per  $\text{nm}^2$ ), which

further increases peptide adsorption without a significant change in  $\zeta$ -potential.<sup>37</sup>

Details of the adsorption mechanism of the peptides as a function of particle size can be inferred from the percentage of time in contact with the surface (Figure 5), conformations in contact with the surface (Figure 6 and SI Movie S1), and the ranked list of proximity of individual residues (SI Table S3). Adsorption of all three peptides increased toward larger particles, that is, toward higher surface ionization at pH  $\sim$  7.4. The variable surface charge of Stöber-type silica particles of different size tunes the adsorption mechanism and selective binding of biomolecules similar to the effect of variable pH (Figure 2).

On the surfaces attributed to the largest particles (210 nm), binding was dominated by electrostatic interactions (Figure 6a, d, g, and SI Table S3). Also, the contribution by hydrogen bonds was significant due to the high total silanol density and surface acidity of the silica surfaces. N-termini of all peptides and the positively charged ammonium group of K1 in KLPGWSG were the primary functional groups that account for peptide adsorption. Hydrogen bonds also involved C-termini in all peptides for significant percentages of time, as well as S6 in KLPGWSG, T6 in AFILPTG, and S7, D2, S4, H3, and H6 in LDHSLHS (SI Table S3). Weaker, intermittent hydrophobic interactions were also observed as a result of peptide exclusion from the solution toward the surface, particularly for the AFILPTG peptide with hydrophobic moieties in the side chains of F2, I3, L4, P5, and T6 residues. Notably, even the negatively charged peptide LDHSLHS was somewhat drawn to the surface, and hydrophobic groups in all peptides remained comparatively distant from the surface due to strong surface-water interactions (see SI Movie S1).

On the surfaces attributed to smaller 82 nm particles, represented by pure  $Q^3$  models with 4.7 SiO(H, Na) and 18% ionization, the significance of ion pairing and hydrogen bonds decreased, resulting in lower affinity of all three peptides (Figure 6b, e, h, and SI Table S3). The most attracted residues are similar to those seen for 210 nm particles; however, the percentage of time anchored and exposed to the surface was reduced. Among the three peptides, the adsorption of AFILPTG on the surface of 82 nm particles showed the largest decrease in binding from  $\sim$ 70% on to  $\sim$ 40% of time in close contact, predominantly associated with the decline in attraction of the peptide N-terminus.

On silica surfaces representing 28 nm nanoparticles, the adsorption of peptide KLPGWSG decreased somewhat further due to less electrostatic attractions. Adsorption of AFILPTG occurred intermittently for  $\sim$ 50% of simulation time primarily mediated by hydrophobic groups, and proximity of LDHSLHS was observed  $\sim$ 40% of simulation time through hydrogen bonds (Figure 6c, f, i). The adsorption mechanism on the surfaces of smaller silica particles involved less ion pairing, less hydrogen bonds, and increasingly hydrophobic interactions, similar to adsorption at low pH.

As mentioned above, the experimentally measured adsorption for the 28 nm samples is substantially lower than the affinity predicted by molecular dynamics simulation on idealized regular surfaces (Figure 5b, c). Thereby, the relative trend in peptide attraction is still consistent between measurements and simulation. The authors believe that structural irregularities (Figure 1a) make much of the internal, nitrogen-accessible surface area in BET measurements unavailable to peptide adsorption, whereby adsorption was nevertheless

reported relative to this surface area (Figure 5, SI Figure S3, and SI section S2). Previous studies also report poor definition and plasticity, as well as incomplete dissociation of organic precursor groups for Stöber-type silica particles smaller than 50 nm.<sup>75</sup> The disproportionately weak adsorption of peptides in experiment (SI Figure S3) may thus be related to overestimated accessible surface area and to the possible presence of some residual hydrophobic organic groups on the silica surface (see more details in SI Table S4 and SI section S4). Certainly, more work is needed to consolidate poorly defined silica nanostructures with representative models.

In summary, computational predictions of biomolecular binding as a function of particle size correlate well with measurements. Close correspondence of true surface chemistry and morphology to the representation in models is thereby essential. The demonstrated sensitivity enables binding predictions for numerous existing and novel silica morphologies, as well as the elucidation of irregular silica structural models consistent with experimental information on structure and binding that often remains incomplete.

#### 4. CONCLUSIONS

In conclusion, specific silica surface models of different degree of ionization were employed to study the adsorption of various peptides as a function of pH and nanoparticle size. Data from adsorption isotherms and from molecular simulation were found to be in very good agreement, showing that the INTERFACE-CHARMM force field and a surface model database<sup>26,37</sup> are suitable to predict selective adsorption in atomic resolution.

The results also reiterate the mechanism of adsorption and rationally explain the contribution of different factors in the context of the surface chemistry and charge states of silica and peptides. The contributions to selective adsorption involve ion pairing, hydrogen bonds, conformation effects, and hydrophobic interactions. A higher pH value in the solution results in higher negative charge density on the silica surface and shifts adsorption toward positively charged peptides, diminishing the attraction of negatively charged peptides, the influence of hydrogen bonds and hydrophobic interactions. pH had little effect on neutral peptides, which were more weakly bound by hydrogen bonds and hydrophobic interactions. At lower pH, binding differentials between all peptides diminish and hydrophobic residues increasingly interact with the surface. Binding of the same peptides to three batches of silica nanoparticles of different diameters showed stronger adsorption on larger particles with higher surface silanol density ( $Q^2/Q^3$  environments), surface ionization, and absence of porosity. Weaker hydrophobic interactions on less ionic surfaces of smaller particles originate from the exclusion of peptides from the aqueous phase to minimize disruptions of the network of hydrogen bonds. The different contributions to binding are tunable in customized proportions and can be evaluated by molecular dynamics simulation. Poor definition and "sponginess" of small (28 nm silica) nanoparticles showed much reduced peptide attraction in experiment, in part related to the limited accessibility of the BET surface area.

While the force field accurately predicts binding of biomolecules for the chosen conditions, the representation of silica surface structure in the models must be handled with care. The feasibility of predictive simulations can be applied to a wide range of surface chemistry and topology, multiplied by a huge number of specific biomolecules and adsorbents, to

engineer silica materials for desired performance at the atomic scale. In combination with new synthesis and characterization methods, computations can reduce the time spent on trial-and-error based chemistry. The models can be applied to screen the binding and release of drug molecules to customized silica nanostructures, evaluate silica nanoparticle interactions with specific receptors on cell surfaces, track the adsorption of gases in silica glasses and zeolites (using complementary parameters for aluminosilicates),<sup>26</sup> and assess the self-assembly of silica nanostructures, polymer and hydrogel composites at given pH, ionic concentration, and temperature.

## ■ ASSOCIATED CONTENT

### Supporting Information

Complete details of computational methods, experimental methods, experimental data for model validation, additional discussion of specific peptide binding, supporting figures and tables, as well as a movie depicting the desorption of peptides from different silica surfaces by steered molecular dynamics simulation. This material is available free of charge via the Internet at <http://pubs.acs.org>.

## ■ AUTHOR INFORMATION

### Corresponding Authors

\*Email: carole.perry@ntu.ac.uk.

\*Email: hendrik.heinz@uakron.edu.

### Notes

The authors declare no competing financial interest.

## ■ ACKNOWLEDGMENTS

We acknowledge support from the Air Force Research Laboratory, UES, Inc., the Air Force Office of Scientific Research (F.S.E. and H.H. via FA8650-09-D-5037, C.C.P. via FA9550-10-1-0024 and FA9550-13-1-0040), the National Science Foundation (DMR-0955071), the University of Akron, and the Ohio Supercomputing Center for the allocation of computational resources.

## ■ REFERENCES

- (1) Hoffmann, F.; Cornelius, M.; Morell, J.; Froba, M. *Angew. Chem., Int. Ed.* **2006**, *45*, 3216–3251.
- (2) Iler, R. K. *The Chemistry of Silica: Solubility, Polymerization, Colloid, and Surface Properties, and Biochemistry*; John Wiley & Sons: New York, 1979.
- (3) Slowing, I. I.; Trewyn, B. G.; Giri, S.; Lin, V. S. Y. *Adv. Funct. Mater.* **2007**, *17*, 1225–1236.
- (4) Mackowiak, S. A.; Schmidt, A.; Weiss, V.; Argyo, C.; von Schirnding, C.; Bein, T.; Bräuchle, C. *Nano Lett.* **2013**, *13*, 2576–2583.
- (5) Hildebrand, M. *Chem. Rev.* **2008**, *108*, 4855–4874.
- (6) Kaehr, B.; Townson, J. L.; Kalinich, R. M.; Awad, Y. H.; Swartzentruber, B. S.; Dunphy, D. R.; Brinker, C. J. *Proc. Natl. Acad. Sci. U.S.A.* **2012**, *109*, 17336–17341.
- (7) Kröger, N.; Lorenz, S.; Brunner, E.; Sumper, M. *Science* **2002**, *298*, 584–586.
- (8) Patwardhan, S. V. *Chem. Commun.* **2011**, *47*, 7567–7582.
- (9) Patwardhan, S. V.; Emami, F. S.; Berry, R. J.; Jones, S. E.; Naik, R.; Deschaume, O.; Heinz, H.; Perry, C. C. *J. Am. Chem. Soc.* **2012**, *134*, 6244–6256.
- (10) Puddu, V.; Perry, C. C. *ACS Nano* **2012**, *6*, 6356–6363.
- (11) Sarthou, G.; Timmermans, K. R.; Blain, S.; Treguer, P. *J. Sea Res.* **2005**, *53*, 25–42.
- (12) Sumper, M.; Brunner, E. *Adv. Funct. Mater.* **2006**, *16*, 17–26.
- (13) Cha, J. N.; Stucky, G. D.; Morse, D. E.; Deming, T. J. *Nature* **2000**, *403*, 289–292.
- (14) Kröger, N.; Deutzmann, R.; Sumper, M. *Science* **1999**, *286*, 1129–1132.
- (15) Muller, W. E. G.; Schroder, H. C.; Burghard, Z.; Pisignano, D.; Wang, X. H. *Chem.—Eur. J.* **2013**, *19*, 5790–5804.
- (16) Patwardhan, S. V.; Clarson, S. J.; Perry, C. C. *Chem. Commun.* **2005**, 1113–1121.
- (17) Perry, C. C.; Patwardhan, S. V.; Deschaume, O. *Biochem. Soc. Trans.* **2009**, *37*, 687–691.
- (18) Rimola, A.; Costa, D.; Sodupe, M.; Lambert, J.-F.; Ugliengo, P. *Chem. Rev.* **2013**, *113*, 4216–4313.
- (19) Stober, W.; Fink, A.; Bohn, E. *J. Colloid Interface Sci.* **1968**, *26*, 62–69.
- (20) Vigil, G.; Xu, Z. H.; Steinberg, S.; Israelachvili, J. *J. Colloid Interface Sci.* **1994**, *165*, 367–385.
- (21) Coppage, R.; Slocik, J. M.; Ramezani-Dakhel, H.; Bedford, N. M.; Heinz, H.; Naik, R. R.; Knecht, M. R. *J. Am. Chem. Soc.* **2013**, *135*, 11048–11054.
- (22) Feng, J.; Pandey, R. B.; Berry, R. J.; Farmer, B. L.; Naik, R. R.; Heinz, H. *Soft Matter* **2011**, *7*, 2113–2120.
- (23) Heinz, H. *Clay Miner.* **2012**, *47*, 205–230.
- (24) Heinz, H.; Castelijns, H. J.; Suter, U. W. *J. Am. Chem. Soc.* **2003**, *125*, 9500–9510.
- (25) Heinz, H.; Koerner, H.; Anderson, K. L.; Vaia, R. A.; Farmer, B. L. *Chem. Mater.* **2005**, *17*, 5658–5669.
- (26) Heinz, H.; Lin, T.-J.; Mishra, R. K.; Emami, F. S. *Langmuir* **2013**, *29*, 1754–1765.
- (27) Heinz, H.; Suter, U. W. *J. Phys. Chem. B* **2004**, *108*, 18341–18352.
- (28) Heinz, H.; Suter, U. W.; Leontidis, E. *J. Am. Chem. Soc.* **2001**, *123*, 11229–11236.
- (29) Mishra, R. K.; Flatt, R. J.; Heinz, H. *J. Phys. Chem. C* **2013**, *117*, 10417–10432.
- (30) Ruan, L.; Ramezani-Dakhel, H.; Chiu, C.-Y.; Zhu, E.; Li, Y.; Heinz, H.; Huang, Y. *Nano Lett.* **2013**, *13*, 840–846.
- (31) Ugliengo, P.; Sodupe, M.; Musso, F.; Bush, I. J.; Orlando, R.; Dovesi, R. *Adv. Mater.* **2008**, *20*, 4579–4583.
- (32) Schneider, J.; Ciacchi, L. C. *J. Am. Chem. Soc.* **2012**, *134*, 2407–2413.
- (33) Wright, L. B.; Walsh, T. R. *Phys. Chem. Chem. Phys.* **2013**, *15*, 4715–4726.
- (34) Calzolari, A.; Cicero, G.; Cavazzoni, C.; Di Felice, R.; Catellani, A.; Corni, S. *J. Am. Chem. Soc.* **2010**, *132*, 4790–4795.
- (35) Heinz, H. *J. Phys.: Condens. Matter* **2014**, *26*, 244105.
- (36) Liu, H.; Espe, M.; Modarelli, D. A.; Arias, E.; Moggio, I.; Ziolo, R. F.; Heinz, H. *J. Mater. Chem. A* **2014**, *2*, 8705–8711.
- (37) Emami, F. S.; Puddu, V.; Berry, R. J.; Varshney, V.; Patwardhan, S. V.; Perry, C. C.; Heinz, H. *Chem. Mater.* **2014**, *26*, 2647–2658.
- (38) Bolt, G. H. *J. Phys. Chem.* **1957**, *61*, 1166–1169.
- (39) Tadros, T. F.; Lyklema, J. *J. Electroanal. Chem. Interfacial Electrochem.* **1968**, *17*, 267–275.
- (40) Zerrouk, R.; Foissy, A.; Mercier, R.; Chevallier, Y.; Morawski, J.-C. *J. Colloid Interface Sci.* **1990**, *139*, 20–29.
- (41) Sonnfeld, J. *J. Colloid Interface Sci.* **1996**, *183*, 597–599.
- (42) Puddu, V.; Perry, C. C. *Langmuir* **2014**, *30*, 227–233.
- (43) Sanders, M. J.; Leslie, M.; Catlow, C. R. A. *J. Chem. Soc., Chem. Commun.* **1984**, 1271–1273.
- (44) van Beest, B. W. H.; Kramer, G. J. *Phys. Rev. Lett.* **1990**, *64*, 1955–1958.
- (45) Hill, J. R.; Sauer, J. *J. Phys. Chem.* **1994**, *98*, 1238–1244.
- (46) Cruz-Chu, E. R.; Aksimentiev, A.; Schulten, K. *J. Phys. Chem. B* **2006**, *110*, 21497–21508.
- (47) Hassanali, A. A.; Singer, S. J. *J. Phys. Chem. B* **2007**, *111*, 11181–11193.
- (48) Hassanali, A. A.; Zhang, H.; Knight, C.; Shin, Y. K.; Singer, S. J. *J. Chem. Theory Comput.* **2010**, *6*, 3456–3471.
- (49) Lopes, P. E. M.; Murashov, V.; Tazi, M.; Demchuk, E.; MacKerell, A. D. *J. Phys. Chem. B* **2006**, *110*, 2782–2792.

- (50) Butenuth, A.; Moras, G.; Schneider, J.; Koleini, M.; Köppen, S.; Meißner, R.; Wright, L. B.; Walsh, T. R.; Ciacchi, L. C. *Phys. Status Solidi B* **2012**, *249*, 292–305.
- (51) Flikkema, E.; Bromley, S. T. *Chem. Phys. Lett.* **2003**, *378*, 622–629.
- (52) Goumans, T. P.; Wander, A.; Brown, W. A.; Catlow, C. R. *Phys. Chem. Chem. Phys.* **2007**, *9*, 2146–2152.
- (53) Skelton, A. A.; Fenter, P.; Kubicki, J. D.; Wesolowski, D. J.; Cummings, P. T. *J. Phys. Chem. C* **2011**, *115*, 2076–2088.
- (54) Garofalini, S. H. *J. Chem. Phys.* **1982**, *76*, 3189–3192.
- (55) Lockwood, G. K.; Garofalini, S. H. *J. Chem. Phys.* **2009**, *131*, 074703.
- (56) Pedone, A.; Malavasi, G.; Menziani, M. C.; Segre, U.; Musso, F.; Corno, M.; Civalleri, B.; Ugliengo, P. *Chem. Mater.* **2008**, *20*, 2522–2531.
- (57) Du, J.; Cormack, A. N. *J. Am. Ceram. Soc.* **2005**, *88*, 2532–2539.
- (58) Gambino, G. L.; Lombardo, G. M.; Grassi, A.; Marletta, G. J. *Phys. Chem. B* **2004**, *108*, 2600–2607.
- (59) Lobel, K. D.; West, J. K.; Hench, L. L. *J. Mater. Sci. Lett.* **1996**, *15*, 648–650.
- (60) Rimola, A.; Civalleri, B.; Ugliengo, P. *Langmuir* **2008**, *24*, 14027–14034.
- (61) Yang, J. J.; Meng, S.; Xu, L. F.; Wang, E. G. *Phys. Rev. B* **2005**, *71*, 035413.
- (62) Oren, E. E.; Notman, R.; Kim, I. W.; Spencer, E. J.; Walsh, T. R.; Samudrala, R.; Tamerler, C.; Sarikaya, M. *Langmuir* **2010**, *26*, 11003–11009.
- (63) Oren, E. E.; Tamerler, C.; Sahin, D.; Hnilova, M.; Seker, U. O. S.; Sarikaya, M.; Samudrala, R. *Bioinformatics* **2007**, *23*, 2816–2822.
- (64) Argyris, D.; Cole, D. R.; Striolo, A. *Langmuir* **2009**, *25*, 8025–8035.
- (65) Feng, J.; Slocik, J. M.; Sarikaya, M.; Naik, R. R.; Farmer, B. L.; Heinz, H. *Small* **2012**, *8*, 1049–1059.
- (66) Fu, Y. T.; Heinz, H. *Chem. Mater.* **2010**, *22*, 1595–1605.
- (67) Heinz, H.; Farmer, B. L.; Pandey, R. B.; Slocik, J. M.; Patnaik, S. S.; Pachter, R.; Naik, R. R. *J. Am. Chem. Soc.* **2009**, *131*, 9704–9714.
- (68) Heinz, H.; Suter, U. W. *Angew. Chem., Int. Ed.* **2004**, *43*, 2239–2243.
- (69) Heinz, H.; Vaia, R. A.; Koerner, H.; Farmer, B. L. *Chem. Mater.* **2008**, *20*, 6444–6456.
- (70) Heinz, H.; Vaia, R. A.; Krishnamoorti, R.; Farmer, B. L. *Chem. Mater.* **2007**, *19*, 59–68.
- (71) Jha, K. C.; Liu, H.; Bockstaller, M. R.; Heinz, H. *J. Phys. Chem. C* **2013**, *117*, 25969–25981.
- (72) Mishra, R. K.; Fernández-Carrasco, L.; Flatt, R. J.; Heinz, H. *Dalton Trans.* **2014**, *43*, 10602–10616.
- (73) Heinz, H. *J. Comput. Chem.* **2010**, *31*, 1564–1568.
- (74) Zhang, L.; D'Acunzi, M.; Kappl, M.; Imhof, A.; van Blaaderen, A.; Butt, H.-J.; Graf, R.; Vollmer, D. *Phys. Chem. Chem. Phys.* **2010**, *12*, 15392–15398.
- (75) Costa, C. A. R.; Leite, C. A. P.; Galembeck, F. *J. Phys. Chem. B* **2003**, *107*, 4747–4755.